Technical Report ECOM-01870-17 November 1967

COMPUTATIONAL UTILITY OF NONLINEAR TRANSISTOR MODELS

C. E. L. Technical Memorandum No. 98

Contract No. DA 28-043-AMC-01870(E)

DA Project No. 1 PO 21101 AO42. 01. 02

Prepared by

Alan B. Macnee

COOLEY ELECTRONICS LABORATORY

Department of Electrical Engineering
The University of Michigan
Ann Arbor, Michigan

for

U. S. Army Electronics Command, Fort Monmouth, N. J.

ABSTRACT

Three nonlinear models for junction transistors are shown to be equivalent, physically. Their differences lie in the state variables employed. The incremental behavior of these models is compared with that of the Hybrid-π and high-frequency tee.

The computational utility of the voltage-controlled and the charged-controlled models are compared for a switching circuit example. If a single model is used to describe the transistor, all models are "strongly" nonlinear in one or more operating regions. In any single operating region, however, an appropriate model choice leads to "almost linear" equations.

TABLE OF CONTENTS

LIST OF ILLUSTRATIONS

LIST OF TABLES

1. INTRODUCTION

This memorandum demonstrates the equivalence of three large signal transistor models: the model used in the NET-1 circuit analysis program, a model used by D. A. Calahan in his computer circuit analysis course, and D. Koehler's charge-control model (Refs. 1, 2, 3). These models differ primarily in the choice made for the controlling, state variables. Despite their equivalence, the differing variable choices can significantly influence the computational utility of these models in particular circumstances.

The "optimum" variable choice depends upon the transistor's operating condition (saturation, linear or cut-off regions) and upon the external circuit. In general computer-aided analysis programs, it may prove impractical to change transistor models in the course of the solution calculations, but such a step is practical and worthwhile in hand calculated solutions.

1.1 Calahan's Voltage-Controlled Model

This model together with the defining nonlinear equations are given in Fig. 1. Equations 1.1 through 1.4 represent first-order effects and will be essential to any large signal analysis. Equations 1.1 and 1.2 give the exponential behavior of an ideal semiconductor junction, and Eqs. 1.3 and 1.4 describe nonlinear capacitances which account for the stored charge associated with each junction. The voltage dependence of the transition capacitances C_{TE} and C_{TC} and of the forward and reverse alphas, indicated by Eqs. 1.5 through 1.8, are often second-order effects. The voltage dependence of the width of the junction transistion (space-charge) regions is responsible for most of these nonlinear effects. For purposes of comparison with other models it is convenient to write out the voltage dependence of the emitter and collector currents.

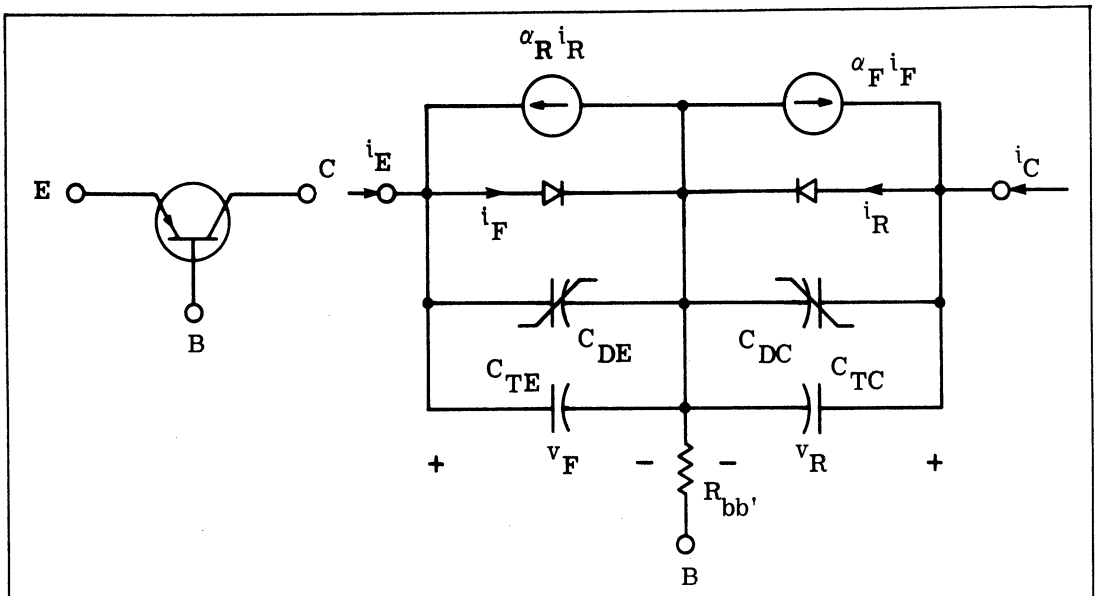

$$i_R = I_{CS}\left(e^{\lambda v_R} - 1\right) \tag{1.1}$$

$$i_F = I_{ES}\left(e^{\lambda v_F} - 1\right) \tag{1.2}$$

$$C_{DE} = \frac{I_{ES}}{\omega_F v_F}\left(e^{\lambda v_F} - 1\right) \tag{1.3}$$

$$C_{DC} = \frac{I_{CS}}{\omega_R v_R}\left(e^{\lambda v_R} - 1\right) \tag{1.4}$$

$$C_{TC} = C_{TC}(v_R) \tag{1.5}$$

$$C_{TE} = C_{TE}(v_F) \tag{1.6}$$

$$\alpha_F = \alpha_F(v_F, v_R) \tag{1.7}$$

$$\alpha_R = \alpha_R(v_F, v_R) \tag{1.8}$$

Fig. 1. Large signal, voltage-controlled transistor model and defining equations

These are

$$i_E = I_{ES}\left(e^{\lambda v_F} - 1\right) + \frac{d}{dt}\left[(C_{TE} + C_{DE})\, v_F\right] - \alpha_R I_{CS}\left(e^{\lambda v_R} - 1\right)$$

$$= I_{ES}\left(e^{\lambda v_F} - 1\right) - \alpha_R I_{CS}\left(e^{\lambda v_R} - 1\right) + \frac{I_{ES}\lambda}{\omega_F} e^{\lambda v_F} \cdot \frac{dv_F}{dt}$$

$$+ \frac{d}{dt}\left(C_{TE}\, v_F\right) \tag{1}$$

and

$$i_C = I_{CS}\left(e^{\lambda v_R} - 1\right) + \frac{d}{dt}\left[(C_{TC} + C_{DC})\, v_R\right] - \alpha_F I_{ES}\left(e^{\lambda v_F} - 1\right)$$

$$= I_{CS}\left(e^{\lambda v_R} - 1\right) - \alpha_F I_{ES}\left(e^{\lambda v_F} - 1\right) + \frac{I_{CS}\lambda}{\omega_R} e^{\lambda v_R} \frac{dv_R}{dt}$$

$$+ \frac{d}{dt}\left(C_{TC}\, v_R\right) . \qquad (2)$$

These equations and Fig. 1 are for the PNP case. For an NPN transistor I_{CS}, I_{ES}, v_R, v_F, should all be multiplied by minus one. The equations are first order, nonlinear, ordinary differential equations in the junction voltages v_F and v_R (v_{EB} and v_{CB}). This model is therefore convenient for node voltage or state-variable formulations of network equilibrium equations. Bulk resistances can easily be included in the emitter and collector leads when they are significant.

It is of interest to examine the incremental behavior predicted by Eqs. 1 and 2, even though one plans to use them for large signal calculations, since numerical integration techniques effectively reduce the nonlinear model to a sequence of linear models. Writing each variable

$$i_E = I_E + i_e$$

$$i_C = I_C + i_c$$

$$v_F = V_{EB} + v_e$$

$$v_R = V_{CB} + v_c$$

as a quiescent value plus an increment, Eqs. 1 and 2 give

$$I_E = I_{ES}\left(e^{\lambda V_{EB}} - 1\right) - \alpha_R I_{CS}\left(e^{\lambda V_{CB}} - 1\right) , \qquad (3)$$

$$I_C = -\alpha_F I_{ES}\left(e^{\lambda V_{EB}} - 1\right) + I_{CS}\left(e^{\lambda V_{CB}} - 1\right), \qquad (4)$$

$$i_e = \left(\lambda I_{ES}\, e^{\lambda V_{EB}}\right)\left(v_e + \frac{1}{\omega_F}\,\frac{dv_e}{dt}\right) + \left(C_{TE} + V_{EB}\,\frac{dC_{TE}}{dv_F}\right)\frac{dv_e}{dt} - \alpha_R\left(\lambda I_{CS}\, e^{\lambda V_{CB}}\right)v_c\,, \tag{5}$$

and

$$i_c = \left(\lambda I_{CS}\, e^{\lambda V_{CB}}\right)\left(v_c + \frac{1}{\omega_R}\,\frac{dv_c}{dt}\right) + \left(C_{TC} + V_{CB}\,\frac{dC_{TC}}{dv_R}\right)\frac{dv_c}{dt} - \alpha_F\left(\lambda I_{ES}\, e^{\lambda V_{CB}}\right)v_e\,. \tag{6}$$

Equations 3 and 4 are the familiar Ebers-Moll equations, relating the quiescent currents to the quiescent voltages (Ref. 4). The incremental Eqs. 5 and 6 are conveniently rewritten as

$$i_e = \frac{1}{r_e}\,v_e + (C_{de} + C_{te})\,\frac{dv_e}{dt} - g_{mr}\,v_c\,, \tag{7}$$

and

$$i_c = \frac{1}{r_c}\,v_c + (C_{dc} + C_{tc})\,\frac{dv_c}{dt} - g_{mf}\,v_e\,; \tag{8}$$

where

$$r_e \triangleq \frac{1}{\lambda I_{ES}\, e^{\lambda V_{EB}}}\,, \tag{9}$$

$$C_{de} \triangleq \frac{1}{\omega_F\, r_e}\,, \tag{10}$$

$$C_{te} \triangleq \left(C_{TE} + V_{EB}\,\frac{dC_{TE}}{dv_F}\right)\Bigg|_{V_{EB}}\,, \tag{11}$$

$$r_c \triangleq \frac{1}{\lambda I_{CS}\, e^{\lambda V_{CB}}}\,, \tag{12}$$

$$C_{dc} \triangleq \frac{1}{\omega_R\, r_c}\,, \tag{13}$$

$$C_{tc} \triangleq \left(C_{TC} + V_{CB} \frac{dC_{TC}}{dv_R} \right) \Bigg|_{V_{CB}} , \tag{14}$$

$$g_{mr} \triangleq \frac{\alpha_R}{r_c} , \tag{15}$$

and

$$g_{mf} \triangleq \frac{\alpha_F}{r_e} . \tag{16}$$

The incremental circuit implied by Eqs. 7 and 8 is given in Fig. 2(a). In the saturation region, this complete model may be required. The relationship between this model and the more common "normal" operation incremental models is illustrated in Figs. 2(b) and (c). If the emitter-base junction is forward biased by at least one-tenth of a volt and the collector-base junction reverse biased by at least the same amount, Eqs. 3 and 4 reduce to

$$I_E = I_{ES} e^{\lambda V_{EB}} + \alpha_R I_{CS} \approx I_{ES} e^{\lambda V_{EB}} , \tag{17}$$

and

$$I_C \approx -\alpha_F I_E - I_{CS}(1 - \alpha_F \alpha_R) . \tag{18}$$

In this region g_{mr}, C_{dc}, and $1/r_c$ all approach zero, and the model reduces to Fig. 2(b) where now

$$r_e = \frac{1}{\lambda I_E} , \tag{19a}$$

$$g_{mf} = \lambda I_E \alpha_F \tag{19b}$$

and

$$C_c \triangleq C_{tc} , \tag{20a}$$

$$C_e \triangleq C_{de} + C_{te} . \tag{20b}$$

If we change the input-controlling variable to $i_1 \triangleq v_e / r_e$, this is seen to be the usual high-frequency T-model without the "excess-phase shift" correction (Ref. 5). On the other hand,

if the model is reoriented, one can easily convert it to the hybrid-π form shown in Fig. 2(c).*

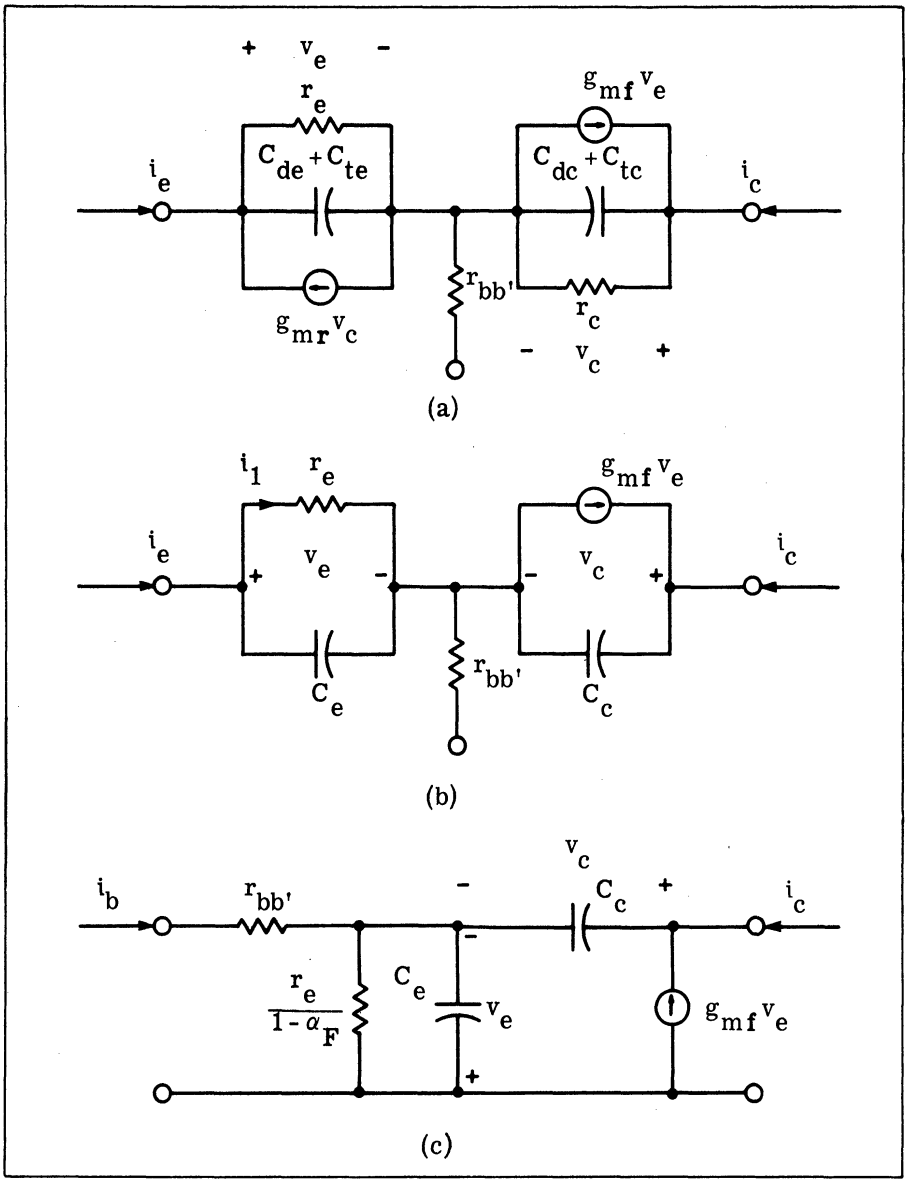

Fig. 2(a) Incremental voltage-controlled model;
(b) Simplified model for "normal" operation; and
(c) Simplified model converted to hybrid-π form

*Here the voltage-controlled current source has been replaced by two equivalent sources, and one of these is converted to the negative conductance of g_{mf} mhos in parallel with r_e.

2. THE NET-1 MODEL

This model and the appropriate defining equations are given in Fig. 3. In comparing this with the voltage-controlled model in Fig. 1 several points can be noted.

The transition capacities in Fig. 3 are assumed to have the specific voltage dependence indicated; the NET-1 user selects three parameters for each capacity. The diffusion capacities in Fig. 3 are incremental values, and they are written as functions of the internal current components i_{CF} and i_{EF}. The choice of incremental values means that the current through the emitter diffusion capacity in Fig. 3 is

$$i_{de} = C_{de} \frac{dv_F}{dt} \quad ,$$

whereas in Fig. 1 the same current is

$$i_{de} = \frac{d}{dt} (C_{TE} v_F) \quad .$$

The NET-1 model includes ohmic bulk resistance in each lead (R_{EE}, R_{BB}, R_{CC}) plus ohmic leakage resistance across each junction (R_E and R_c). This model also introduces two emission constants M_E and M_C to allow for junction voltages and incremental resistances which are greater than predicted by the ideal $e^{\lambda v}$ factor.

The equivalence between the NET-1 model and the voltage-controlled model is established by writing the emitter and collector currents in Fig. 3 as a function of v_F and v_R for the case of R_E and R_C infinite. Kirchhoff's current law at the emitter node gives

$$i_E = i_1 + C_{de} \frac{dv_F}{dt} + \frac{d}{dt} (C_{te} v_F) \quad . \tag{21}$$

Now, substituting Eqs. 3.3 and 3.4 into Eqs. 3.1 and 3.5; and then using Eq. 3.1 to eliminate i_1 in Eq. 21 gives

$$i_E = \frac{I_{EO}}{1-\alpha_F\alpha_R}\left(e^{\frac{\lambda v_F}{M_E}} - 1\right) - \frac{\alpha_R I_{CO}}{1-\alpha_F\alpha_R}\left(e^{\frac{\lambda v_R}{M_C}} - 1\right)$$

$$+\left(\frac{\lambda I_{EO}}{M_E \omega_F (1-\alpha_F\alpha_R)}\, e^{\frac{\lambda v_F}{M_E}}\right)\frac{dv_1}{dt} + \frac{d}{dt}(C_{te} v_F) \quad . \tag{22}$$

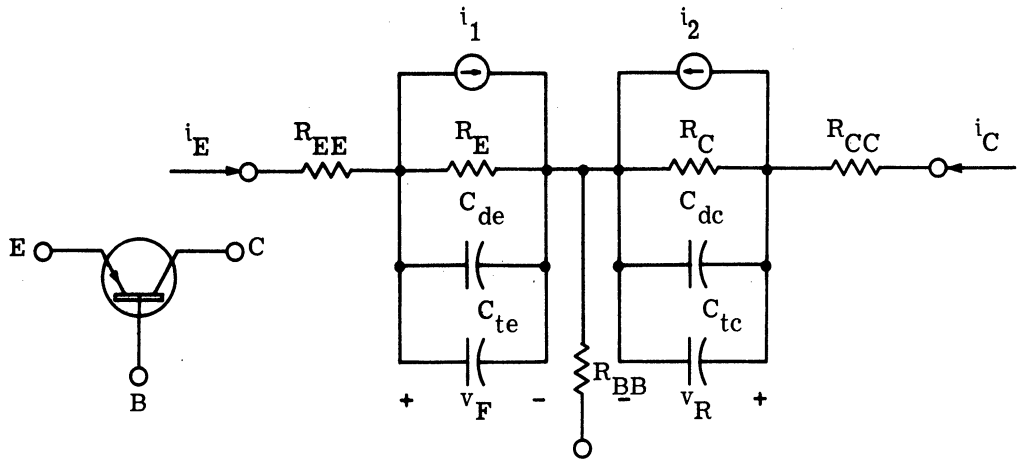

$$i_1 = i_{EF} - \alpha_R i_{CF} \tag{3.1}$$

$$i_2 = i_{CF} - \alpha_F i_{EF} \tag{3.2}$$

$$i_{EF} = \frac{I_{EO}}{1-\alpha_R\alpha_F}\left[e^{\frac{\lambda v_F}{M_E}} - 1\right] \tag{3.3}$$

$$i_{CF} = \frac{I_{CO}}{1-\alpha_R\alpha_F}\left[e^{\frac{\lambda v_R}{M_C}} - 1\right] \tag{3.4}$$

$$C_{de} = \frac{\lambda}{M_E\omega_F}\left[i_{EF} + \frac{I_{EO}}{1-\alpha_R\alpha_F}\right] \tag{3.5}$$

$$C_{dc} = \frac{\lambda}{M_C\omega_R}\left[i_{CF} + \frac{I_{CO}}{1-\alpha_R\alpha_F}\right] \tag{3.6}$$

$$C_{te} = D_1/(V_{ZE} - v_F)^{N_E} \tag{3.7}$$

$$C_{tc} = D_2/(V_{ZC} - v_R)^{N_C} \tag{3.8}$$

$$\alpha_F = \alpha_F(v_F) \tag{3.9}$$

$$\alpha_R = \alpha_R(v_R) \tag{3.10}$$

Fig. 3. Large signal, transistor model used in NET-1 analysis program

Similarly one finds for the collector current

$$i_C = \frac{I_{CO}}{1-\alpha_F\alpha_R}\left(e^{\frac{\lambda v_R}{M_C}} - 1\right) - \frac{\alpha_F I_{EO}}{1-\alpha_F\alpha_R}\left(e^{\frac{\lambda v_F}{M_E}} - 1\right)$$

$$+\left(\frac{\lambda I_{CO}}{M_C \omega_R(1-\omega_F\omega_R)} e^{\frac{\lambda v_R}{M_C}}\right)\frac{dv_R}{dt} + \frac{d}{dt}(C_{tc} v_R) \quad . \tag{23}$$

If we let $M_E = M_C = 1$, and write

$$I_{ES} \triangleq \frac{I_{EO}}{(1-\alpha_F\alpha_R)} \tag{24}$$

$$I_{CS} \triangleq \frac{I_{CO}}{(1-\alpha_F\alpha_R)} \quad , \tag{25}$$

Equations 22 and 23 are identical with Eqs. 1 and 2.

As presented in Fig. 3, the NET-1 model is neither voltage- or current-controlled. The current sources i_1 and i_2 are controlled by two current variables i_{EF} and i_{CF} (which are proportional to the normal and inverse minority-carrier charge densities in the base region) as are the diffusion-capacities; but the transition capacities and the current gains are written as functions of the voltages. If Eqs. 3.3 and 3.4 are used to eliminate the voltages v_F and v_R in Eqs. 3.7 through 3.10, then one is left with a model which is completely current-controlled. Since the controlling currents are proportional to stored charge, this is also the charge-controlled model.

3. THE CHARGE-CONTROLLED MODEL

Koehler's charge-controlled equivalent circuit and defining equations are shown in Fig. 4. In this circuit the relationships equivalent to Eqs. 3.5 and 3.6 or Eqs. 1.3 and 1.4 have been replaced by stores S_N and S_I. These new circuit elements are defined by two relations: (1) the voltage across the store is always zero and (2) the current flow through the store, out of the straight-line side, is the rate of change of the stored charge [$q_N(t)$ and $q_I(t)$ in this circuit]. The normal and inverse alphas α_{N_o} and α_{I_o} can be considered constants or expressed as functions of q_N and q_I.

The currents i_E and i_C are obtained by applying Kirchhoff's current law at the emitter and collector nodes.

$$i_E = \frac{dq_N}{dt} + \frac{q_N}{\tau_{EN}} - \alpha_{I_o} \frac{q_I}{\tau_{CI}} + \frac{d}{dt}(C_{TE} v_F) \quad , \tag{26}$$

and

$$i_C = \frac{dq_I}{dt} + \frac{q_I}{\tau_{CI}} - \alpha_{N_o} \frac{q_N}{\tau_{EN}} + \frac{d}{dt}(C_{TC} v_R) \quad . \tag{27}$$

Comparing these equations with Eqs. 22 and 23 or Eqs. 1 and 2 for the previous models, one is struck by their simplicity and "lack" of nonlinearity. If the alphas are assumed constant, the only nonlinear terms which affect the system dynamics are due to the currents flowing to the transition capacities C_{TE} and C_{TC}. In the saturation region v_F and v_R can be expected to be relatively constant (they will change only 26 millivolts for a 2.3:1 change in q_I or q_N); hence these nonlinear current terms often will be negligible. As q_N and q_I pass through zero, however, these currents become the dominant ones. The beauty of Koehler's charge-controlled model is the simplicity and linearity of Eqs. 26 and 27 in the saturation region. Its equivalence with the voltage-controlled model of Fig. 1 is easily demonstrated by using Eqs. 4.1 and 4.2 to eliminate q_N and q_I in Eqs. 26 and 27. Solving Eqs. 4.1 and 4.2 for q_N and q_I gives

$$q_N(t) = \frac{I_{Eo}\tau_{EN}}{1 - \alpha_{N_o}\alpha_{I_o}}\left(e^{\lambda v_F} - 1\right) \tag{28}$$

$$q_I(t) = \frac{I_{CO}\tau_{CI}}{1 - \alpha_{N_o}\alpha_{I_o}}\left(e^{\lambda v_R} - 1\right) . \tag{29}$$

Differentiating Eq. 28 and then substituting into Eq. 26 one obtains

$$i_E = \lambda I_{ES}\tau_{EN} e^{\lambda v_F} \cdot \frac{dv_F}{dt} + I_{ES}\left(e^{\lambda v_F} - 1\right) - \alpha_{I_o} I_{CS}\left(e^{\lambda v_R} - 1\right) + \frac{d}{dt}\left(C_{TE} v_F\right) , \tag{30}$$

and similarly for Eq. 27

$$i_C = \lambda I_{CS}\tau_{CI} e^{\lambda v_R} \cdot \frac{dv_R}{dt} + I_{CS}\left(e^{\lambda v_R} - 1\right) - \alpha_{N_o} I_{ES}\left(e^{\lambda v_F} - 1\right) + \frac{d}{dt}\left(C_{TC} v_R\right) . \tag{31}$$

If

$$\tau_{EN} \triangleq \frac{1}{\omega_F} \tag{32}$$

$$\tau_{CI} \triangleq \frac{1}{\omega_R} \tag{33}$$

$$\alpha_{N_o} \triangleq \alpha_F \tag{34}$$

$$\alpha_{I_o} \triangleq \alpha_R , \tag{35}$$

these equations are identical with Eqs. 1 and 2. Further, comparing Eqs. 28 and 29 with Eqs. 1. 1 and 1. 2 one sees

$$q_N \triangleq \tau_{EN} i_F = \frac{i_F}{\omega_F} \tag{36}$$

$$q_I \triangleq \tau_{CI} i_R = \frac{i_R}{\omega_R} \tag{37}$$

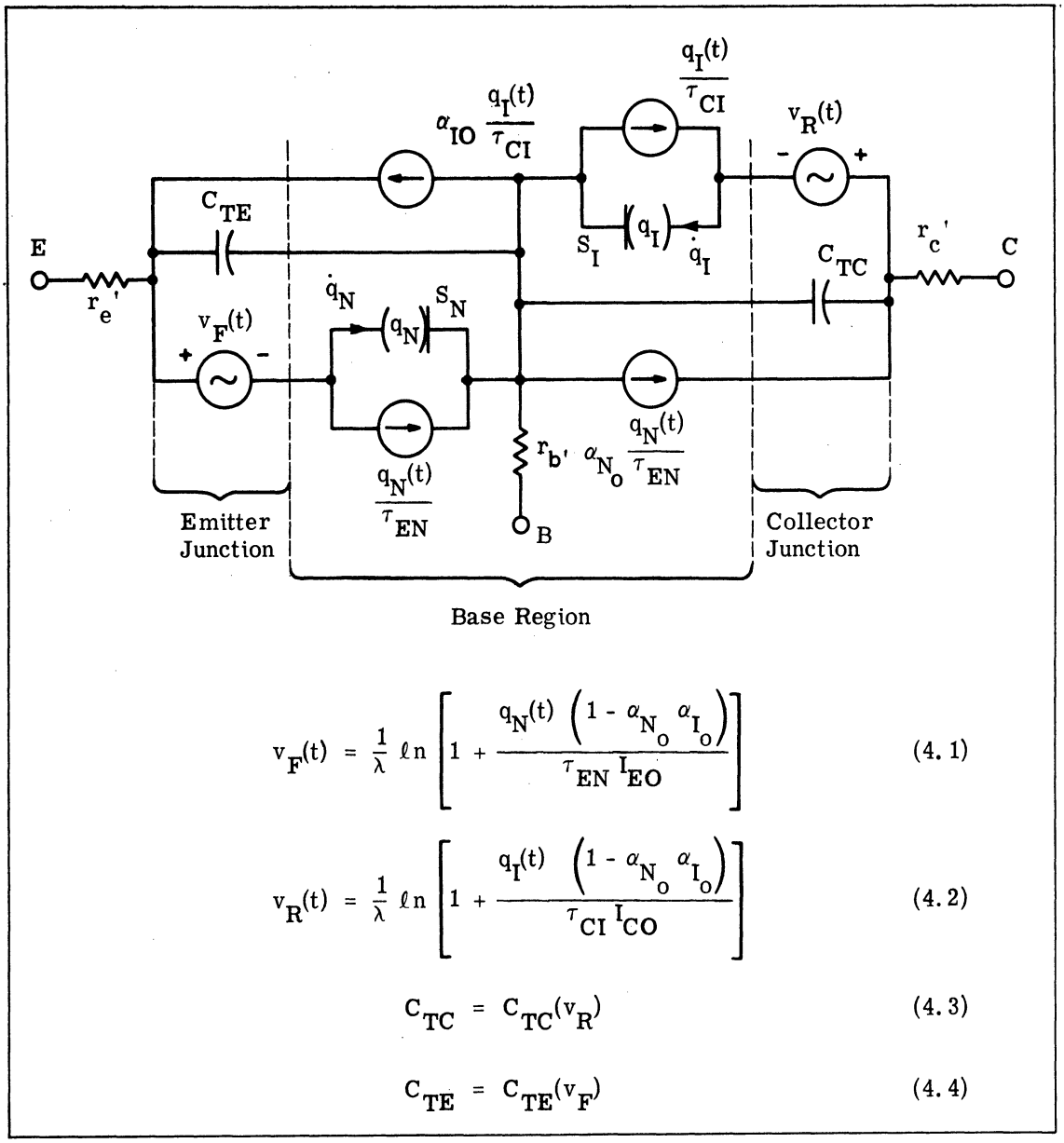

$$v_F(t) = \frac{1}{\lambda} \ell n \left[1 + \frac{q_N(t) \left(1 - \alpha_{N_o} \alpha_{I_o} \right)}{\tau_{EN} I_{EO}} \right] \tag{4.1}$$

$$v_R(t) = \frac{1}{\lambda} \ell n \left[1 + \frac{q_I(t) \left(1 - \alpha_{N_o} \alpha_{I_o} \right)}{\tau_{CI} I_{CO}} \right] \tag{4.2}$$

$$C_{TC} = C_{TC}(v_R) \tag{4.3}$$

$$C_{TE} = C_{TE}(v_F) \tag{4.4}$$

Fig. 4. Charge-control, large signal equivalent circuit

Making the usual split of the dependent variables into quiescent and incremental values, Eqs. 26 and 27 can be split into two sets of equations

$$I_E = \frac{Q_N}{\tau_{EN}} - \alpha_{I_o} \frac{Q_I}{\tau_{CI}} \quad , \tag{38}$$

$$I_C = -\alpha_{N_o} \frac{Q_N}{\tau_{EN}} + \frac{Q_I}{\tau_{CI}} \quad ; \tag{39}$$

and

$$i_e = \frac{dq_n}{dt} + \frac{q_n}{\tau_{EN}} - \alpha_{I_o} \frac{q_i}{\tau_{CI}} + C_{te} \frac{dv_e}{dt} , \tag{40}$$

$$i_c = \frac{dq_i}{dt} + \frac{q_i}{\tau_{CI}} - \alpha_{N_o} \frac{q_n}{\tau_{CN}} + C_{te} \frac{dv_c}{dt} . \tag{41}$$

Similarly expanding Eqs. 4.1 and 4.2 in power series and retaining only two terms gives

$$V_{EB} = \frac{1}{\lambda} \ell n \left[1 + \frac{Q_N(1 - \alpha_{N_o} \alpha_{I_o})}{\tau_{EN} I_{EO}} \right] \tag{42}$$

$$V_{CB} = \frac{1}{\lambda} \ell n \left[1 + \frac{Q_I(1 - \alpha_{N_o} \alpha_{I_o})}{\tau_{CI} I_{CO}} \right] , \tag{43}$$

and

$$v_e = r_e \cdot \frac{q_n}{\tau_{EN}} \tag{44}$$

$$v_c = r_c \cdot \frac{q_i}{\tau_{CI}} , \tag{45}$$

where

$$r_e \triangleq \frac{1}{\lambda \left(\frac{Q_N}{\tau_{EN}} + \frac{I_{EO}}{1 - \alpha_{N_o} \alpha_{I_o}} \right)} \approx \frac{\tau_{EN}}{\lambda Q_N} . \tag{46}$$

and

$$r_c \triangleq \frac{1}{\lambda \left(\frac{Q_I}{\tau_{CI}} + \frac{I_{CO}}{1 - \alpha_{N_o} \alpha_{I_o}} \right)} \approx \frac{\tau_{CI}}{\lambda Q_I} . \tag{47}$$

In Eqs. 40 and 41, C_{te} and C_{tc} are as defined in Eqs. 11 and 14.

Equations 38 and 39 emphasize the linear relationship between the stored charges and the external currents while Eqs. 42 and 43 exhibit the usual logarithmic dependence of the voltages upon these charges. Using Eqs. 42 and 43 to eliminate Q_N/τ_{EN} and Q_I/τ_{CI} in Eqs. 38 and 39 yields the familiar Ebers-Moll Eqs. 3 and 4.

If we let

$$i_1 \triangleq \frac{q_n}{\tau_{EN}} \tag{48}$$

$$i_2 \triangleq \frac{q_i}{\tau_{CI}} \quad , \tag{49}$$

Equations 40, 41, 44 and 45 can be combined into

$$i_e = \frac{1}{r_e} v_e + \left(\frac{\tau_{EN}}{r_e} + C_{te}\right) \frac{dv_e}{dt} - \alpha_{I_o} i_2 \tag{50}$$

and

$$i_c = \frac{1}{r_c} v_c + \left(\frac{\tau_{CI}}{r_c} + C_{tc}\right) \frac{dv_c}{dt} - \alpha_{N_o} i_1 \ . \tag{51}$$

Comparing these equations with Eqs. 7 and 8, taking cognizance of Eqs. 32 through 35, and Eqs. 10 and 13, one sees that they correspond exactly with the exception of the "cross-coupling terms" which are voltage controlled in Eqs. 7 and 8 and current controlled in Eqs. 50 and 51. The incremental model implied by Eqs. 50 and 51 is given in Fig. 5(a). In the special case of "normal" operation this reduces to the high-frequency "T" circuit shown in Fig. 5(b). Here, as in Fig. 2, the diffusion and transition incremental capacities have been combined into single elements C_e and C_c.

Comparing the normal operation, incremental models of Figs. 2(c) and 5(b)

with commonly used incremental models one observes two omissions: (1) base width modulation effects [$r_{b'c}$ and r_{ce} in Fig. 2(c) and r_c and the μv_c generator in Fig. 5(b)], and (2) an excess-phase shift factor. It should be recognized, however, that the large

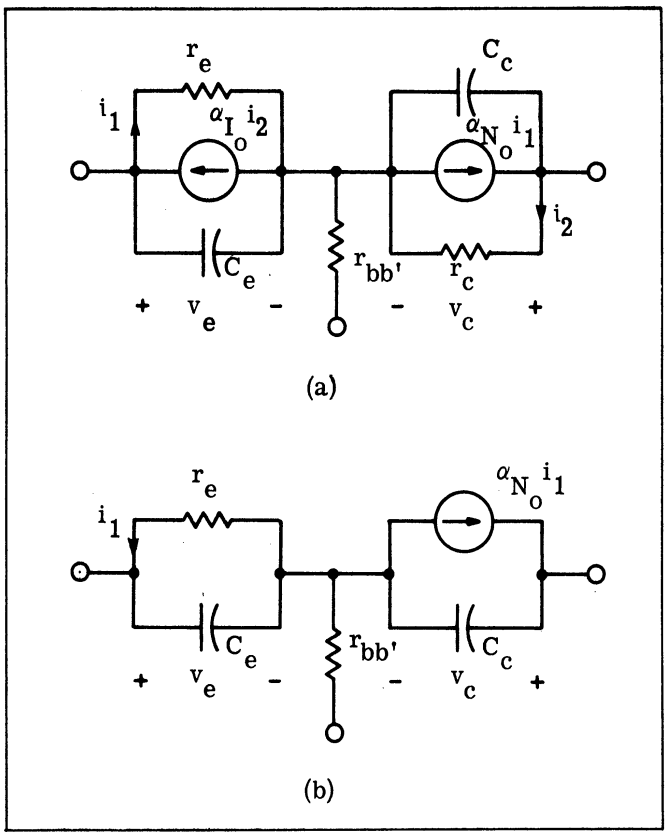

Fig. 5(a) Incremental current-controlled model and
(b) Simplified model for "normal" operation region

$$\left(\frac{Q_I}{\tau_{CI}} \rightarrow \frac{I_{CO}}{1 - \alpha_{N_o}\alpha_{I_o}}\right)$$

signal models will include the major base width modulation effects, if the voltage dependence of the alphas is included. For example, when this is done in the charge-controlled model, the incremental Eqs. 40, 41, 44, and 45 become

$$i_e = \frac{dq_n}{dt} + \frac{q_n}{\tau_{EN}} - \alpha_{I_o}\frac{q_i}{\tau_{CI}} + C_{te}\frac{dv_e}{dt} - \frac{Q_I}{\tau_{CI}}\left(\frac{\partial \alpha_{I_o}}{\partial v_F} v_e + \frac{\partial \alpha_{I_o}}{\partial v_R} \cdot v_c\right), \qquad (40a)$$

$$i_c = \frac{dq_i}{dt} + \frac{q_i}{\tau_{CI}} - \alpha_{N_o} \frac{q_n}{\tau_{EN}} + C_{tc} \frac{dv_c}{dt} - \frac{Q_N}{\tau_{EN}} \left(\frac{\partial \alpha_{N_o}}{dv_R} v_c + \frac{\partial \alpha_{N_o}}{\partial v_F} \cdot v_e \right), \quad (41a)$$

$$v_e = r_e \cdot \frac{q_n}{\tau_{CN}} + \frac{-1}{\lambda \left(1 - \alpha_{N_o} \alpha_{I_o}\right)} \frac{\partial \left(\alpha_{N_o} \alpha_{I_o}\right)}{\partial v_R} \cdot v_c \,, \quad (44a)$$

and

$$v_c = r_c \cdot \frac{q_i}{\tau_{CI}} + \frac{-1}{\lambda \left(1 - \alpha_{N_o} \alpha_{I_o}\right)} \cdot \frac{\partial \left(\alpha_{N_o} \alpha_{I_o}\right)}{\partial v_F} \cdot v_e \,. \quad (45a)$$

The new terms in Eqs. 40a and 41a can be represented in the model of Fig. 5(a) by slight changes in the values of r_e, r_c, α_{N_o} and α_{I_o}, and they are usually negligible when the junction in question is forward biased. In the normal operating region, however, Eq. 41(a) reduces to

$$i_c = -\alpha_{N_o} \frac{q_n}{\tau_{EN}} + C_{tc} \frac{dv_c}{dt} - \frac{Q_N}{\tau_{EN}} \cdot \frac{\partial \alpha_{N_o}}{\partial v_C} \cdot v_c \,. \quad (41b)$$

which can be written

$$i_c = -\alpha_{N_o} i_1 + C_{tc} \frac{dv_c}{dt} + \frac{1}{r_c'} v_c \,, \quad (52)$$

where*

$$r_c' \triangleq \frac{-1}{\frac{Q_N}{\tau_{EN}} \left(\frac{\partial \alpha_{N_o}}{\partial v_R} \right)} = \frac{-1}{I_E \left(\frac{\partial \alpha_{N_o}}{\partial v_R} \right)} \,. \quad (53)$$

This is the usual collector resistance of the low frequency T-model; it is typically in the megohm range and varies inversely as the quiescent emitter current I_E (Ref. 6).

The added terms in Eqs. 44(a) and 45(a) can be represented by voltage-controlled

---

* Recall Eqs. 26, 27, 4.1 and 4.2 are all written for a PNP device and therefore $\frac{\partial \alpha_{N_o}}{\partial v_R}$ is negative.

voltage sources in series with r_e and r_c in Fig. 5(a). These generators will have negligible effect when the junctions are reverse biased, but their influence can be observed at the forward-biased junctions. In the normal operating region, for example, Eq. 44(a) is usually written

$$v_e = r_e i_1 + \mu_{ec} v_c \quad , \tag{54}$$

where

$$\mu_{ec} \triangleq \frac{1}{\lambda\left(1 - \alpha_{N_o} \alpha_{I_o}\right)} \cdot \frac{-\partial\left(\alpha_{N_o} \alpha_{I_o}\right)}{\partial v_R} \quad . \tag{55}$$

To the extent that the diffusion processes, in the base region, are linear μ_{ec}, r_c', r_e and α_{N_o} are related by the equation

$$\frac{\mu_{ec} r_c'}{r_e} = \frac{\alpha_{N_o}}{1 - \alpha_{N_o}^2} \quad . \tag{56}$$*

Figure 6(a) gives the "normal" T incremental equivalent circuit when these space-charge-layer widening effects are included. If the alpha voltage dependences are included in the voltage controlled circuit, the complete hybrid-π circuit shown in Fig. 6(b) results. Equivalently the hybrid-π model parameters can be derived directly from the T-model of Fig. 6(a) (Refs 7, 8). The relations are

$$r_{b'e} = \frac{r_e}{1 - \alpha_{N_o}} \quad , \tag{57}$$

$$r_{ce} = \frac{r_e}{\mu_{ec}} \quad , \tag{58}$$

$$g_m = \frac{\alpha_{N_o} - \mu_{ec}}{r_e} \approx \frac{\alpha_{N_o}}{r_e} \quad , \tag{59}$$

---

*This useful relationship is pointed out in the Mullard Reference Manual of Transistor Circuits, 1st edition, 1960, pp. 82-83; but it does not appear to be very generally recognized.

$$r_{b'c} = \frac{r_c'}{1 - \frac{\mu_{ec}(1-\alpha_{N_o})r_c'}{r_e}} \approx r_c'(1+\alpha_{N_o}) \quad , \tag{60}$$

$$C_{b'c} = C_c \quad , \tag{61}$$

and

$$C_{b'e} = C_e \quad . \tag{62}$$

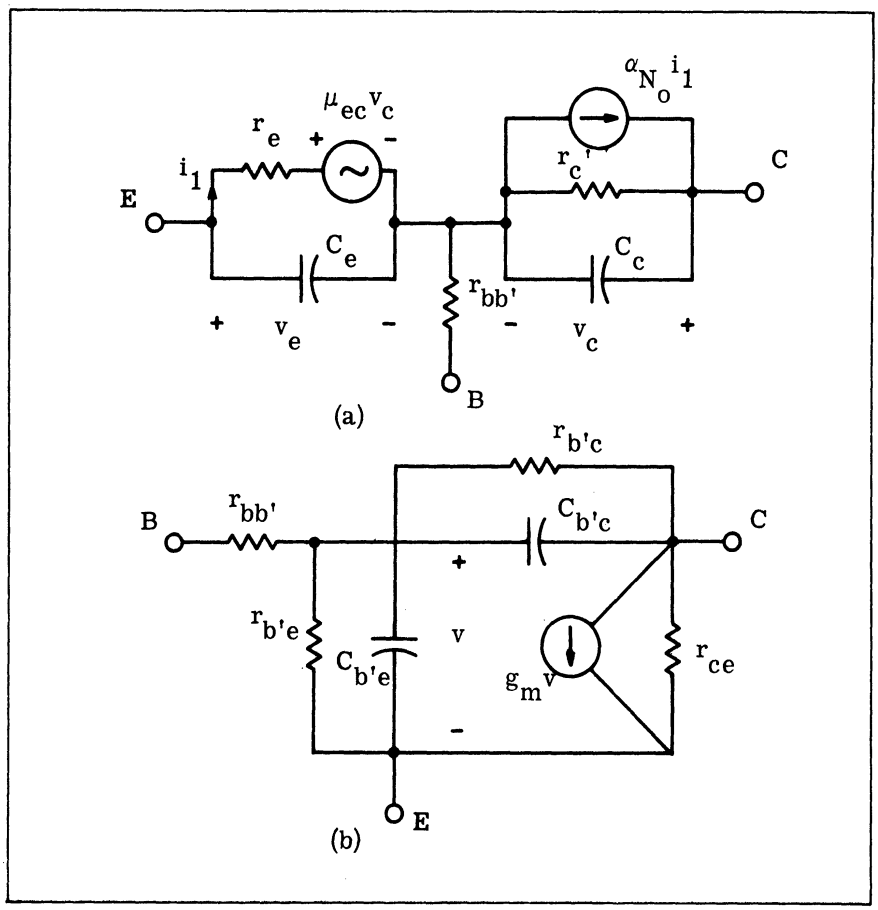

Fig. 6. T and hybrid-π equivalent circuits including base-width modulation effects

The one effect all of these large signal models ignore is the excess-phase shift factor. At the incremental model level, Fig. 6(a), this effect may be approximately included by multiplying α_{N_o} by a pure phase shift factor.*

*m is a real constant which usually is in the range 0.25 to 1.0.

$$\alpha_{N_o} \rightarrow \alpha_{N_o} \, e^{-\frac{ms}{\omega_F}} \quad . \tag{63}$$

When this is done and the T-model is converted to the hybrid-π, only the values of g_m and $C_{b'e}$ are modified;

$$g_m = \frac{\alpha_{N_o}}{r_e} \, e^{-\frac{ms}{\omega_F}} \quad , \tag{59a}$$

and

$$C_{b'e} \simeq C_e(1 + m\,\alpha_{N_o}) \quad . \tag{62a}$$

The excess-phase shift correction given in Eq. 63 represents a pure time delay of $m/\omega_F = m\,\tau_{EN}$ seconds. This effect could be introduced into the large signal models by delaying the transfer current generators. For example, in Fig. 1, the current-controlled current generator would be

$$\begin{aligned} \alpha_R \, i_R(t) &\rightarrow \alpha_R \, i_R\left(t - \frac{m_R}{\omega_R}\right) \\ \alpha_F \, i_F(t) &\rightarrow \alpha_F \, i_F\left(t - \frac{m_F}{\omega_F}\right) \end{aligned} \tag{64}$$

and in Fig. 4

$$\begin{aligned} \alpha_{I_o} \cdot \frac{q_I(t)}{\tau_{CI}} &\rightarrow \alpha_{I_o} \cdot \frac{q_I\,(t - m_R\tau_{CI})}{\tau_{CF}} \\ \alpha_{N_o} \cdot \frac{q_N(t)}{\tau_{EN}} &\rightarrow \alpha_{N_o} \cdot \frac{q_N(t - m_F\tau_{EN})}{\tau_{EN}} \quad . \end{aligned} \tag{65}$$

One can reach some general conclusions about all three large signal models. First, they are essentially equivalent, differing only in the choice of controlling, or state, variables. It will be shown in the next section that this may not be a trivial difference in large signal calculations.

Secondly, if fixed values are assumed for the normal and inverse alphas, all models neglect base-width modulation and excess-phase shift effects. When the voltage

dependence of the alphas is introduced, the predominant base-width modulation effects are reproduced.* The excess-phase shift effects could be included by adding suitable time delays in the appropriate transfer current generators which represent the collected currents.

To the writer's knowledge workers in the area of large signal transistor circuits have not added the excess-phase, time delays. If the analysis program employed is a time domain program, this should be relatively easy to do, and it would appear that the effects might well be significant for fast switching circuits and high-frequency high power amplifiers or oscillators.

---

*This is the normal capability in the NET-1 model, for example.

4. CHOICE OF A LARGE SIGNAL MODEL

The relative merits of various incremental models of junction transistors have been discussed at great length in the literature* (Refs. 7 and 9). The two most popular models are the hybrid-pi and the high-frequency tee. Despite the protestations of various writers concerning the fundamental nature of one model or the other, there can be a complete equivalence between their two models. This equivalence is given in the previous section in Fig. 6 plus Eqs. 57 through 62(a). Each model, in its greatest generality, contains eight parameters which are related rather directly to physical processes in the transistor. At the higher frequencies two parameters μ_{ce} and r_c', in Fig. 6(a) and $r_{b'c}$ and r_{ce} in Fig. 6(b) can be neglected, leaving only six parameters. For those applications which are insensitive to the excess-phase shift, only five parameters are left in either model; and in each case one of these is predictable without measurement (r_e and g_m).

For large signal analyses, as has been pointed out, two models have been used which correspond closely to these small signal cases. The large signal version of the tee model is the charge-controlled tee model, and the large signal version of the hybrid-π is the voltage-controlled model. These two large signal models are equivalent, and one should expect them to yield the same results if the nonlinear differential equations are solved exactly. In practice, however, such equations are usually integrated numerically. Such a solution involves breaking down the nonlinear equations into a sequence of linear equations. The allowable "step" size in such an approximate solution can vary markedly between the two "equivalent" models. This difference can reflect directly into cost per computation run and hence can be of considerable engineering importance.

To illustrate these general remarks a specific example will be used. The

*R. L. Pritchard, loc. cit., gives an excellent summary as of 1956; see also Elementary Circuit Properties of Transistors, SEEC, Vol. 3, Wiley, 1964, pp. 212-217.

circuit in Fig. 7 is one which is commonly specified for measurement of the storage time of a switching transistor. Assuming the circuit has reached equilibrium in the saturated condition before t = 0, the problem is to calculate the storage and turn-off transients. For this example, the transistor parameters are taken to be

$$\alpha_F = 0.98 = \alpha_{N_o}$$

$$\alpha_R = 0.50 = \alpha_{I_o}$$

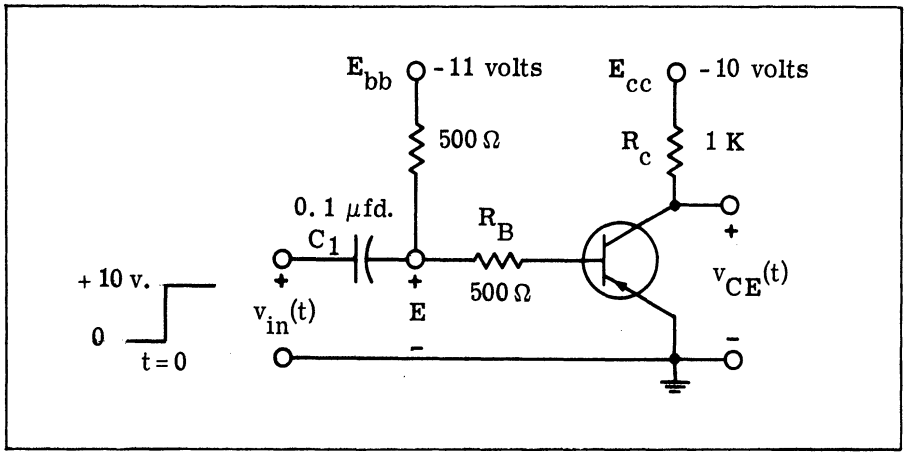

Fig. 7. Switching transistor test circuit

$$\omega_F = \omega_R = 10^9 \text{ rad/sec} = \frac{1}{\tau_{CI}} = \frac{1}{\tau_{EN}}$$

$$C_{TC} = C_{TE} = 2 \text{ pf}$$

$$I_{CS} = I_{ES} = 10^{-8} \text{ amps}$$

For simplicity both the alphas and the transition capacities are taken as constants.

4.1 Voltage-Controlled Model in Saturation Region

Using the voltage-controlled model of Fig. 1, with v_R and v_F as the dependent state variables, the equilibrium equations are obtained by writing Kirchhoff's current law at the collector and the emitter:

$$\left(C_{TC} + \frac{I_{CS}\lambda}{\omega_R} e^{\lambda v_R}\right) \frac{dv_R}{dt} = -I_{CS}\left(e^{\lambda v_R} - 1\right) + \alpha_F I_{ES}\left(e^{\lambda v_F} - 1\right) + \frac{v_F + E_{CC} - v_R}{R_C} \tag{66}$$

and

$$\left(C_{TE} + \frac{I_{ES}\lambda}{\omega_F} e^{\lambda v_F}\right) \frac{dv_F}{dt} = -I_{ES}\left(e^{\lambda v_F} - 1\right) + \alpha_R I_{CS}\left(e^{\lambda v_R} - 1\right) + \frac{v_R - v_F - E_{CC}}{R_C} - \frac{v_F + E_{th}}{R_{th}} \quad . \tag{67}$$

Here E_{th} is the Thevenin voltage seen looking into the external circuit from the base-emitter terminals of the transistor, and R_{th} is the Thevenin resistance at the same point. In the steady state, prior to $t=0$, $E_{th} = -11$ volts and $R_{th} = 1000$ ohms. When $v_{in}(t)$ jumps to +10 volts, the Thevenin voltage is 10 minus the initial voltage on the coupling capacitor; and the Thevenin resistance is 500 ohms.

These equations have been integrated numerically for the particular case presented in Fig. 7.* The initial equilibrium values were found by a Newton-Raphson solution of the equations with the derivatives set to zero and with $E_{th} = -11$ volts and $R_{th} = 1000$ ohms. Taking $\lambda = 40$ volts^{-1}, the initial values are

$$v_F(0^-) = 373 \text{ mv}$$

$$v_R(0^-) = 363 \text{ mv}$$

$$v_{C_1}(0^-) = -5.687 \text{ volts} \quad .$$

Therefore for $t \geq 0$

*This problem was assigned by Prof. D. A. Calahan as part of his course in computer analysis of electrical networks; the writer used solutions obtained by N. E. Abbott and R. J. Talsky.

$$E_{th} = +4.313 \text{ volts} ,$$

and $R_{th} = 500\Omega$. (The change in v_{c_1} is negligible for the times of interest.) Writing $v_F(t)$ and $v_R(t)$ as these initial values plus changes $v_f(t)$ and $v_r(t)$, Eqs. 66 and 67 reduce to

$$\frac{dv_r}{dt} = \frac{-20.06\, e^{40v_r} + 30.01\, e^{40v_f} + v_f - v_r - 9.99}{\left(2 + 804\, e^{40v_r}\right) \times 10^{-9}} , \tag{66a}$$

and

$$\frac{dv_f}{dt} = \frac{-30.07\, e^{40v_f} + 10.03\, e^{40v_r} + v_r - 3v_f + 0.618}{\left(2 + 1228\, e^{40v_f}\right) \times 10^{-9}} , \tag{67a}$$

where now $v_f(0+) = v_r(0+) = 0$. Table I summarizes the results of some numerical integrations of Eqs. 66(a) and 67(a) for the first two nanoseconds of the solution. The first three pairs of columns give the results of Euler integration with time-step sizes of 1, 0.5, and 0.2 nanoseconds. The last pair of columns give the results of a Runge-Kutta integration with a 0.1 nanosecond time step, and this is taken as the "exact" solution. Since the exponential terms decrease 9.5 percent every time v_f or v_r change by 2.5 millivolts, it is clearly desirable to choose a step size small enough to limit Δv_r and Δv_f to this value or less. Here a uniform Δt of 0.1 nanosecond would probably be adequate for most purposes. A more sophisticated integration--such as the Runge-Kutta method--allows much larger step sizes; in this example, a step as large as 1 nanosecond did not seriously change the Runge-Kutta result.

4.2 Charge Controlled Model in Saturation Region

Consider now the same example using the charge controlled model of Fig. 4. Again, the appropriate equilibrium equations can be obtained by applying Kirchhoff's current law at the collector and the emitter terminals.

	Euler Integration						Runge-Kutta	
	$\Delta t = 1$		$\Delta t = 0.5$		$\Delta t = 0.2$		$\Delta t = 0.1$	
t in Nanoseconds	v_r	v_f	v_r	v_f	v_r	v_f	v_r	v_f
0	0	0	0	0	0	0	0	0
0.1								
0.2					-0.010	- 3.158	- 0.432	- 3.154
0.3								
0.4					-0.90	- 6.083	- 1.558	- 6.128
0.5			- 0.0249	- 7.895			- 2.325	- 7.561
0.6					-2.395	- 8.947	- 3.210	- 8.966
0.7								
0.8					-4.371	-11.567	- 5.300	-11.712
0.9								
1.0	- 0.0497	-15.78	- 5.080	-14.173	-6.827	-14.111	- 7.759	-14.401
1.1								
1.2								
1.3								
1.4								
1.5			-12.160	-20.066			-15.557	-21.077
1.6								
1.7								
1.8								
1.9								
2.0	-18.49	-23.86					-26.256	-28.033

All voltages are in millivolts

Table I. Numerical integration of Eqs. 66(a) and 67(a)

$$\left(1 + \frac{C_{TC}}{\lambda(q_I + I_{CS}/\omega_R)}\right) \frac{dq_I}{dt} =$$

$$- \omega_R q_I + \alpha_F \omega_F q_N + \frac{E_{CC} + \frac{1}{\lambda} \ell n \left[\frac{1 + \frac{q_N \omega_F}{I_{ES}}}{1 + \frac{q_I \omega_R}{I_{CS}}}\right]}{R_C} , \qquad (68)$$

and

$$\left(1 + \frac{C_{TE}}{\lambda(q_N + I_{ES}/\omega_F)}\right) \frac{dq_N}{dt} =$$

$$- \omega_F q_N + \alpha_R \omega_R q_I - \frac{E_{CC} + \frac{1}{\lambda} \ell n \left[\frac{1 + \frac{q_N \omega_F}{I_{ES}}}{1 + \frac{q_I \omega_R}{I_{CS}}}\right]}{R_C} - \frac{E_{th} + \frac{1}{\lambda} \ell n \left[1 + \frac{q_N \omega_F}{I_{ES}}\right]}{R_B} . \quad (69)$$

In writing Eqs. 68 and 69, Eqs. 32 through 35, 24 and 25 have been used to make the comparison with Eqs. 66 and 67 evident. On the face of things, one might conclude that there is little to choose between Eqs. 68, 69, or Eqs. 66 and 67; both are rather "messy" pairs of nonlinear differential equations. Notice, however, that the importance of the nonlinear terms depends on the operating range. For example, the only nonlinear term on the right-hand side of Eq. 68 is simply the collector-emitter voltage divided by R_C. Clearly, this term will be negligible in the saturation region ($q_I > 0$). On the right side of Eq. 69 an additional nonlinear term is just v_{EB}/R_B, and we know that even a 100:1 change in $q_N(t)$ will only require a 100 millivolt change in v_{BE}. The same exponential law which produced such rapid changes in the coefficients of Eqs. 66 and 67 with voltage, is working for us!

The only other nonlinearities in Eqs. 68 and 69 are in the coefficients of dq_I/dt and dq_N/dt. These nonlinear effects will be negligible provided

$$q_I(t) >> \frac{C_{TC}}{\lambda} - \frac{I_{CS}}{\omega_R} \quad (70)$$

and

$$q_N(t) >> \frac{C_{TE}}{\lambda} - \frac{I_{ES}}{\omega_F} \quad (71)$$

For the problem at hand $C_{TC}/\lambda = C_{TE}/\lambda = 5 \times 10^{-14}$ coulombs while I_{CS}/ω_R and I_{ES}/ω_F are both 10^{-17} coulombs. Further, the initial values of the stored charges are

$$q_N(0^-) = \frac{I_{ES}}{\omega_F}\left(e^{\lambda v_F(0^-)} - 1\right) = 3.07 \times 10^{-11} \text{ coulombs}$$

and

$$q_I(0^-) = \frac{I_{CS}}{\omega_R}\left(e^{\lambda v_R(0^-)} - 1\right) = 2.01 \times 10^{-11} \text{ coulombs}$$

Conditions in Eqs. 70 and 71 imply that the storage (or diffusion-capacity) current is much greater than the transition capacity current. In the present example the stored charges can drop to one percent of their initial values before the transition capacitors represent five percent of the total.

In summary, while the voltage-controlled Eqs.66 and 67 are very nonlinear in the saturation region, the charge-controlled equations, are almost linear! The fact that the storage time can be calculated closely, by solving linear differential equations was pointed out orginally by J. L. Moll (Ref. 10).

In the present example, writing the stored charges as their initial values plus changes $q_n(t)$ and $q_i(t)$ and substituting the numerical values reduces Eqs. 68 and 69 to

$$\frac{dq_i}{dt} = \frac{-q_i + 0.98\, q_n + 2.5 \times 10^{-14} \ell n \left(\dfrac{3.07 \times 10^{-11} + q_n}{2.01 \times 10^{-11} + q_i}\right)}{\left(1 + \dfrac{2.49 \times 10^{-3}}{1 + \dfrac{q_i}{2.01 \times 10^{-11}}}\right) \times 10^{-9}} \tag{68a}$$

and

$$\frac{dq_n}{dt} = \frac{-q_n + 0.5q_i - 1.928\times10^{-11} - 2.5\times10^{-14} \ell n \left(\dfrac{3.07\times10^{-11} + q_n}{2.01\times10^{-11} + q_i}\right) - 5\times10^{-14} \ell n(3.07\times10^{6} + 10^{17} q_n)}{\left(1 + \dfrac{1.629 \times 10^{-3}}{1 + \dfrac{q_n}{3.07 \times 10^{-11}}}\right)} \tag{69a}$$

Linear approximations to these equations are

$$10^9 \frac{dq_i}{dt} = -q_i + 0.98\, q_n \tag{68b}$$

and

$$10^9 \frac{dq_n}{dt} = -q_n + 0.5 q_i - 2.005 \times 10^{-11} \quad . \tag{69b}$$

Solving these linear equations with the specified initial value one finds

$$q_i(t) = (-3.849 + 4.674\, e^{-0.3t} - 0.825\, e^{-1.7t}) \times 10^{-11} \text{ coulombs} \tag{72}$$

and

$$q_n(t) = (-3.927 + 3.338\, e^{-0.3t} + 0.589\, e^{-1.7t}) \times 10^{-11} \text{ coulombs} \tag{73}$$

for $|q_i(t)| > 0.0201 \times 10^{-11}$ coulombs and t in nanoseconds. Table II compares these solutions with the results of the Runge-Kutta Integration of Eqs. 66(a) and 67(a).

The voltages are related to the charges by Eqs. 4.1 and 4.2 which for the present problem reduce to

$$v_f = 25\ell n \left(1 + \frac{10^{11} q_n}{3.07}\right)$$

and

$$v_r = 25\ell n \left(1 + \frac{10^{11} q_i}{2.01}\right)$$

In calculating Table II a slide rule was used to evaluate the necessary exponentials and logarithms. Clearly, the agreement between the numerical integration of the nonlinear equations of the voltage-controlled formulation and the linear approximation to the charge-controlled equations is excellent over the saturation region of operation. For this example, the transistor remains saturated for 3.1 nanoseconds.

Linear Approximation Eqs. 68(b) and 69(b) Solutions					Runge-Kutta Integration of Eqs. 66(a) and 67(a)	
	Charge in Picacoulombs Voltage in mv				Voltage in mv	
Time in Nanoseconds	$q_i(t)$	$q_n(t)$	v_r	v_f	v_r	v_f
0	0	0	0	0	0	0
0.2	- 0.3443	- 3.639	- 0.434	- 3.153	- 0.432	- 3.154
0.4	- 1.213	- 6.677	- 1.556	- 6.13	- 1.558	- 6.128
0.6	- 2.418	- 9.260	- 3.200	- 8.91	- 3.210	- 8.966
0.8	- 3.849	-11.503	- 5.315	-11.76	- 5.300	-11.712
1.0	- 5.362	-13.460	- 7.760	-14.42	- 7.759	-14.40
1.2	- 6.957	-15.218	-10.620	-17.11	-10.591	-17.06
1.4	- 8.546	-16.794	-13.83	-19.77	-13.80	-19.73
1.6	-10.101	-18.220	-17.46	-22.50	-17.43	-22.43
1.8	-11.646	-19.547	-21.65	-25.35	-21.55	-25.19

Table II. Comparison of linear charge-controlled and nonlinear voltage-controlled equation solutions

4.3 The Linear and Cut-Off Regions

4.3.1 Using Voltage-Controlled Model. The previous sections have compared the voltage-controlled and the charge-controlled transistor models for calculations in the saturation region. In this region the charge-controlled equations are "almost" linear whereas the voltage-controlled equations are "strongly" nonlinear.

It is illuminating to continue the comparison of the two models into the normal, or linear operating region. In this region: v_R and q_I are less than zero, but v_R and q_N are still positive. The voltage-controlled Eqs. 66(a) and 67(a) and the charge-controlled Eqs. 68(a) and 69(a) are written in terms of incremental voltages and charges. At the "edge" of the linear region

$$v_r(t) = -0.363 \text{ volts}$$

and

$$q_i(t) = -2.01 \times 10^{-11} \text{ coulombs} .$$

The Runge-Kutta integration of Eqs. 66(a) and 67(a) gives for the time to reach this point (the storage time)

$$T_s = 3.23 \text{ nanosec} ,$$

and at this time

$$v_f(3.20) = 0.0492 \text{ volts}$$

and therefore

$$q_n(3.23) = -2.64 \times 10^{-11} \text{ coulombs} .$$

As the operating point moves into the linear region, $v_r(t)$ is going to become more negative, and therefore the terms in Eqs. 66a and 67a which depend exponentially on $v_r(t)$ are negligible. These equations then reduce to

$$\frac{dv_r}{dt} = \frac{30.01\, e^{40v_f} + v_f - v_r - 9.99}{2 \times 10^{-9}} , \tag{67b}$$

and

$$\frac{dv_f}{dt} = \frac{-30.07\, e^{40v_f} + v_r - 3v_f + 0.618}{\left(2 + 1228\, e^{40v_f}\right) \times 10^{-9}} . \tag{66b}$$

These are still "strongly" nonlinear in v_f, but no difficulty is to be expected if the numerical integrations, begun in the saturation region, are continued into the linear region. The edge of the "cut-off" region is defined by the point

$$v_f(t) = -0.373 \text{ volts} .$$

This solution of Eqs. 66(a) and 66(b) reaches this point at t = 4.69 monoseconds, and

$$v_r(4.69) = -4.63 \text{ volts} .$$

This is less than half way to the cut-off equilibrium value of -10 volts! This brings out a point, which does not seem to have been recognized in the literature; there can be a substantial difference between the time required to reach "cut-off," as defined by both junctions being reverse biased, and the time needed to bring the collector current down to 10 percent of its saturation value.

For times greater than 4.69 nanoseconds the remaining exponential terms in Eqs. 66(b) and 67(b) become negligible, and the voltage-controlled equations reduce to the pair of linear equations

$$\frac{dv_r}{dt} = \frac{v_f - v_r - 9.99}{2 \times 10^{-9}} , \tag{66c}$$

and

$$\frac{dv_f}{dt} = \frac{v_f - 3v_f + 0.618}{2 \times 10^{9}} . \tag{67c}$$

These equations are linear because of the assumption, for this example, that the transition capacities C_{TC} and C_{TE} are constants. The expected voltage dependence of these capacities would make the equations nonlinear.

Continuing the integration of Eqs. 66(c) and 67(c) one finds that the collector current reaches -1 milliampere at $t = 10.7$ nanoseconds. Therefore the turn-off time for the collector current is $10.7 - 3.2 = 7.5$ nanoseconds while the transistor junction cut-off time is only $4.69 - 3.23 = 1.46$ nanoseconds!

4.3.2 Using Charge-Controlled Model. Turning to the charge-controlled Eqs. 68(a) and 69(a) as

$$q_i(t) \rightarrow -2.01 \times 10^{-11} \text{ coulombs}$$

one would expect that the linear approximation Eqs. 68(b) and 69(b) would no longer be valid, since two of the neglected logarithmic terms in Eqs. 68(a) and 69(a) approach infinity! Nevertheless, solving Eq. 72 for the time required for $q_i(t)$ to reach -2.01×10^{-11} $(1 - 0.498 \times 10^{-6})$ coulombs (this corresponds to $v_r = 0.363$ volts or $v_R = 0$) gives

$$T_s = 3.16 \text{ nanoseconds}$$

and at this time, Eq. 73 gives

$$q_n(3.16) = -2.61 \times 10^{-4} \text{ coulombs} .$$

These values agree very closely with those obtained from the numerical solution of Eqs. 66(a) and 67(a). Thus, the linear approximations, Eqs. 68(b) and 69(b), are seen to be useful right up to the very edge of the linear region. Certainly it is unreasonable to expect Eqs. 68(b) and 69(b) to continue to be accurate in the linear region. If one chooses to continue the solutions with the charges as state variables, the resulting nonlinear equations must be integrated numerically.

4.3.3 Combined-Voltage and Charge-Control. An alternative, at this point, is to go back and make a new selection of variables. Returning to Fig. 4, as $q_I(t)$ becomes negligible, Kirchhoff's current law at the collector node of the charge controlled model gives (see Eq. 27)

$$-i_C = \frac{\alpha_{N_o}}{\tau_{EN}} q_N(t) - \frac{d}{dt} (C_{TC} v_R) \tag{74}$$

and at the emitter node

$$-i_C - i_B = \frac{dq_N}{dt} + \frac{q_N}{\tau_{EN}} + \frac{d}{dt} (C_{TE} v_F) . \tag{75}$$

In the circuit of Fig. 7

$$i_C = \frac{-v_R + v_F + E_{CC}}{R_C} , \tag{76}$$

and

$$i_B = \frac{E_{th} + v_F}{R_{th}} . \tag{77}$$

As long as the transistor is in the normal, or forward operating region, 0.324 volts $< v_F <$ 0. Over most of this region v_F will lie withing 50 millivolts of

0.324 volts. This suggests neglecting the change of v_F in this region. When this is done, Eqs. 74 through 77 reduce to

$$\frac{d}{dt}\left(C_{TC}\, v_R\right) + \frac{v_R}{R_c} - \frac{\alpha_{N_o}}{\tau_{EN}}\, q_N(t) = \frac{E_{CC} + 0.324}{R_c} \quad , \tag{78}$$

and

$$\frac{dq_N}{dt} + \frac{1}{\tau_{EN}}\, q_N(t) - \frac{v_R}{R_c} = \frac{-E_{CC} - 0.324}{R_c} + \frac{-E_{th} - 0.324}{R_{th}} \quad . \tag{79}$$

For the present example, C_{TC} is a constant, and these equations are linear in the variables $v_R(t)$ and $q_N(t)$. Introducing numerical values gives

$$\frac{dv_R}{dt'} + 0.5 \times 10^9\, v_R - 0.49 \times 10^{21}\, q_N = -4.8384 \times 10^9 \quad , \tag{78a}$$

and

$$\frac{dq_N}{dt'} + 10^9\, q_N - 10^{-3}\, v_R = 4.02 \times 10^{-2} \quad ; \tag{79a}$$

with initial conditions $v_R(0+) = 0$, and $q_N(0+) = 3.07 - 2.61 = 0.46 \times 10^{-11}$ coulombs.* The solutions of this pair of equations are

$$10^{12}\, q_N(t') = -463.7 + 467.559\, e^{-\frac{t'}{150}} + 0.741\, e^{-\frac{3}{2}t'} \quad \text{coulombs} \tag{80}$$

and

$$v_R(t') = -464.1 + 464.441\, e^{-\frac{t'}{150}} - 0.341\, e^{-\frac{3}{2}t'} \quad \text{volts} \tag{81}$$

where t' is expressed in nanoseconds. Equations 78 and 79, and hence their solutions, apply as long as $q_N(t') > 0$. Using Eq. 80 one finds that $q_N(t')$ reaches zero at $t' = 1.27$ nanoseconds, and

$$v_R(1.27) = -3.65 \text{ volts} \quad .$$

*Here, the time origin has been shifted to the instant at which the transistor enters the "linear" region. This is 3.23 nanoseconds after the application of the base voltage step.

This "cut-off time" is 15 percent shorter than the value calculated by the voltage-controlled Eqs. 66 and 67, and the voltage drop is about 27 percent less. It is clear that over this traversal of the transistor's normal operating region the exponential, $\exp\left(\frac{t'}{150}\right)$, in Eqs. 80 and 81 is well approximated by the first two terms in its power series expansion so that

$$10^{12}\, q_N(t') \approx 3.859 - 3.117\, t' + 0.711\, e^{-\frac{3}{2}t'} \tag{82}$$

and

$$v_R(t') \approx -3.096\, t' + 0.341\left(1 - e^{-\frac{3}{2}t'}\right) \tag{83}$$

as long as $0 \leqq t' \leqq 1.5$.

These solutions predict an almost linear time dependence for both $q_N(t)$ and $v_R(t)$. This essentially linear time behavior is observed in the voltage-controlled equation solutions. Beyond $t = 3.23 + 1.27 = 4.5$ nanoseconds, the assumption of a fixed v_F is no longer valid and as a result, Eq. 4.1 must be used to eliminate v_F in Eq. 75. The result is a nonlinear differential equation in $q_N(t)$.

However, the voltage-controlled Eqs. 66 and 67, in the cut-off region became linear

$$2 \times 10^{-9} \frac{dv_R}{dt''} + v_R - v_F = -10 \tag{66d}$$

and

$$2 \times 10^{-9} \frac{dv_F}{dt''} + 3v_F - v_R = 1.687 \quad . \tag{67d}$$

The solutions of these equations with the initial conditions $v_R(0) = -3.65$ and $v_F(0) = 0.324$ are

$$v_R(t'') = -14.313 + 10.582\, e^{-0.2929t''} + 0.081\, e^{-1.7071t''} \text{ volts}, \tag{84}$$

and

$$v_F(t'') = -4.313 + 4.4489\, e^{-0.2929t''} + 0.1881\, e^{-1.7071t''} \text{ volts}. \qquad (85)$$

The collector-emitter voltage is the difference of these two junction voltages

$$v_{CE}(t'') = -10 + 6.133\, e^{-0.2929t''} - 0.107\, e^{-1.7071t''} \text{ volts} \qquad (86)$$

In all three of these solutions t'' is the time in nanoseconds measured from the instant at which $v_R(t) = 0$. Equation 86 is a direct indication of $i_C(t)$ since $v_{CE} = E_{CC} - i_C R_C$. Equation 86 predicts the time required for i_c to reach -1.0 ma, t'' = 6.19 nanoseconds, which corresponds to a total time t = 4.5 + 6.19 = 10.69 nanoseconds from the time of application of the base voltage pulse. Figure 8 summarizes the numerical example presented here. The solid curves are plots of the numerical integration of the voltage-controlled nonlinear equations, and the crosses represent the values obtained with the three linear sets of equations.

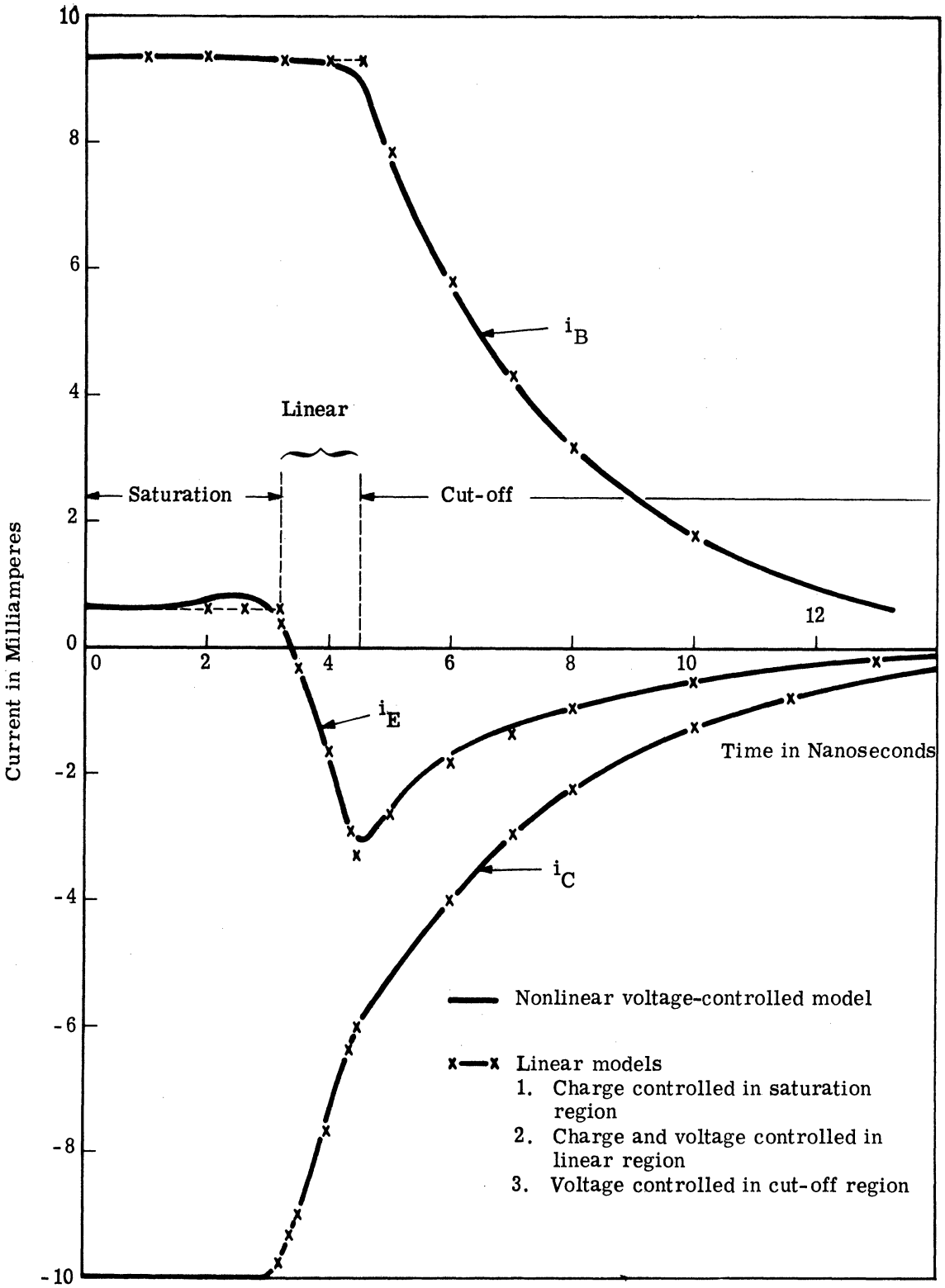

Fig. 8 Calculated current response of saturated transistor (see Fig. 7)

5. SUMMARY

The example of Sec. 4 brings into focus some of the situations which may be encountered when a particularly large signal transistor model is used to predict circuit behavior over a wide range of operating conditions. This example carries the transistor through all three operating regions: saturation, normal (or linear), and cut-off. If one wishes to describe the transistor by a single model, then either the voltage-controlled or the charge-controlled models lead to "strongly" nonlinear differential equations over two of the three operating regions. In the saturation region the voltage-controlled formulation leads to strongly nonlinear equations while the charge-controlled equations are "almost" linear. In the cut-off region the voltage-controlled equations are almost linear, and the charge-controlled equations are strongly nonlinear. Finally in the normal operating region both the charge-controlled and the voltage-controlled models yield strongly nonlinear differential equations. In this region, however, one can obtain a set of almost linear equations by choosing as variables one charge and one voltage (q_N and v_R).

In computer analysis programs one may prefer a single model for all regions of operation. This makes the analysis of nonlinear differential equations inevitable. If one is willing to change models, whenever a transistor transitions from cut-off-to-normal or normal-to-saturation, for example; then three linear models may be accurate enough for many calculations. The linear models are particularly attractive when hand calculations are involved and in giving the circuit designer a "feel" for the circuit behavior.

REFERENCES

1. Electronic Design, Vol. 15, No. 12, June 7, 1967, pp. 57-59 or A. F. Mahnberg, F. Q. Cornwell, and F. N. Hofer, NET-1 Network Analysis Program, 7090/94 Version, LA3119, Los Almos Scientific Laboratory, Los Almos, New Mexico, 1964.

2. D. A. Calahan, Notes on Computer Analysis of Circuits, Winter-Term 1967, University of Michigan, Ann Arbor, Michigan.

3. Dankwark Koehler, "The Charge-Control Concept in the Form of Equivalent Circuits, ...," B. S. T. J., Vol. XLVI, No. 3, March 1967, pp. 523-576.

4. J. J. Ebers and J. L. Moll, "Large Signal Behavior of Junction Transistors," Proc. IRE, XLII, December 1954, pp. 1761-1772.

5. M. V. Joyce and K. K. Clarke, Transistor Circuit Analysis, Addison-Wesley Pub. Co., (96), pp. 231-233.

6. J. M. Early, "Effects of Space-Charge-Layer Widening in Junction Transistors," Proc. IRE, Vol. 40, November 1952, pp. 1401-1405.

7. R. L. Pritchard, "Electric-Network Representations of Transistors - A Survey," IRE Trans. Circuit Theory, Vol. CT-3, pp. 5-21.

8. Mullard Reference Manual of Transistor Circuits, 1st Edition, 1960, pp. 83-84.

9. Elementary Circuit Properties of Transistors, SEEC, Vol. 3, Wiley, 1964, pp. 212-217.

10. J. L. Moll, "Large-Signal Transient Response of Junction Transistors," Proc. IRE, Vol. 42, December 1954, pp. 1773-1783.

DISTRIBUTION LIST

No. of Copies	
10	Defense Documentation Center Attn: DDC-IRS Cameron Station (Bldg. 5) Alexandria, Virginia 22314
1	Office of Assistant Secretary of Defense (Research and Engineering) Attn: Technical Library, Rm 3E1065 Washington, D. C. 20301
1	Defense Intelligence Agency Attn: DIARD Washington, D. C. 20301
1	Bureau of Ships Technical Library Attn: Code 312 Main Navy Bldg., Rm 1528 Washington, D. C. 20325
1	Chief, Bureau of Ships Attn: Code 454 Department of the Navy Washington, D. C. 20360
2	Director U. S. Naval Research Lab. Attn: Code 2027 Washington, D. C. 20390
1	Commanding Officer and Director U. S. Navy Electronics Lab. Attn: Library San Diego, California 92101
1	Commander U. S. Naval Ordnance Lab. Attn: Technical Library White Oak, Silver Spring, Maryland 20910
1	AFSC STLO (RTSND) Naval Air Development Center Johnsville, Warminster, Pennsylvania 18974
1	Rome Air Development Center (EMTLD) Attn: Documents Library Griffiss Air Force Base New York 13440

No. of Copies	
1	Systems Engineering Group (SEPIR) AVWW Wright-Patterson Air Force Base Ohio 45433
2	Electronic Systems Div. (ESTI) L. G. Hanscom Field Bedford, Massachusetts 01731
1	Air Proving Ground Ctr (PGBPS-12) Attn: PGAPI Eglin Air Force Base, Florida 32542
1	Air University Library (3T) Maxwell Air Force Base Alabama 36112
2	Chief of Research & Development Department of the Army Washington, D. C. 20315
2	Commanding General U. S. Army Materiel Command Attn: R&D Directorate Washington, D. C. 20315
1	Commanding General U. S. Army Combat Developments Command Attn: CDCMR-E Fort Belvoir, Virginia 22060
3	Commanding Officer U. S. Army Combat Developments Command Communications-Electronics Agency Fort Monmouth, New Jersey 07703
1	Commanding Officer U. S. Army Sec Agcy Combat Dev Actv Arlington Hall Station Arlington, Virginia 22212
1	U. S. Army Secutiry Agency Attn: OACofS, DEV (CDA) Arlington Hall Station Arlington, Virginia 22212
1	Harry Diamond Laboratories Attn: Library Connecticut Ave. & Van Ness St. Washington, D. C. 20438

DISTRIBUTION LIST (Cont.)

No. of Copies	
1	Asst Secretary of the Army (R&D) Department of the Army Attn: Deputy Asst for Army (R&D) Washington, D. C. 20315
1	Asst Secretary of the Army (R&D) Department of the Army Attn: Asst for Research Washington, D. C. 20315
1	Commanding Officer U. S. Army Limited War Lab. Aberdeen Proving Ground, Maryland 21005
2	C. G. U. S. Army Security Agcy Attn: IALOG and IARD Arlington Hall Station Arlington, Virginia 22207
1	Stanford Electronics Labs. Stanford University Attn: Dr. D. G. Grace Stanford, California
1	Chief, Mountain View Office Electronic Warfare Lab. USAECOM P. O. Box 205 Mountain View, California 94042
1	Chief, Intelligence Materiel Dev Office Electronic Warfare Lab. USAECOM Fort Holabird, Maryland 21219
1	Chief Missile Electronic Warfare Tech Area EW Lab, USA Electronics Com White Sands Missile Range New Mexico 88002
1	Chief, Willow Run Office CSTA Lab. USAECOM P. O. Box 618 Ann Arbor, Michigan 48107
1	Headquarters U. S. Army Combat Developments Command Attn: CDCLN-EL Fort Belvoir, Virginia 22060

No. of Copies	
1	USAECOM Liaison Officer MIT, Bldg 26, Rm 131 77 Massachusetts Avenue Cambridge, Massachusetts 02139
1	USAECOM Liaison Officer Aeronautical Systems Division Attn: ASDL-9 Wright-Patterson AFB, Ohio 45433
1	USAECOM Liaison Officer Rome Air Development Center Attn: EMPL Griffiss Air Force Base, New York 13440
1	USAECOM Liaison Office U. S. Army Electronic Proving Ground Fort Huachuca, Arizona 85613
1	Director NSA Ft. George G. Meade, Maryland
1	Dr. T. W. Butler, Jr., Director Cooley Electronics Laboratory The University of Michigan Ann Arbor, Michigan 48105
6	Cooley Electronics Laboratory The University of Michigan Ann Arbor, Michigan 48105
15	Commanding General U. S. Army Electronics Command Ft. Monmouth, New Jersey 07703 Attn: AMSEL-EW WL-D WL-S WL-N WL-C WL-E HL-CT-DD RD-MAT RD-MAF RD-MAF-2 RD-GFR XL-D RD-LNA KL-TM

UNCLASSIFIED

Security Classification

DOCUMENT CONTROL DATA - R&D

(Security classification of title, body of abstract and indexing annotation must be entered when the overall report is classified)

1. ORIGINATING ACTIVITY (Corporate author) Cooley Electronics Laboratory The University of Michigan Ann Arbor, Michigan	2a. REPORT SECURITY CLASSIFICATION UNCLASSIFIED 2b. GROUP

3. REPORT TITLE

COMPUTATIONAL UTILITY OF NONLINEAR TRANSISTOR MODELS

4. DESCRIPTIVE NOTES (Type of report and inclusive dates)

7695-17-T (TM 98) - November 1967

5. AUTHOR(S) (Last name, first name, initial)

Macnee, Alan B.

6. REPORT DATE	7a. TOTAL NO. OF PAGES	7b. NO. OF REFS
November 1967		10

8a. CONTRACT OR GRANT NO.	9a. ORIGINATOR'S REPORT NUMBER(S)
DA 28-043-AM-01870(E) b. PROJECT NO. PO 21101 A042. 01. 02 c. d.	C. E. L. TM 98 9b. OTHER REPORT NO(S) (Any other numbers that may be assigned this report) ECOM-01870-17-T

10. AVAILABILITY/LIMITATION NOTICES This document is subject to special export controls and each transmittal to foreign governments or foreign nationals may be made only with prior approval of CG, U.S. Army Electronics Command, Fort Monmouth, N. J. 07703 Attn: AMSEL-WL-S.

11. SUPPLEMENTARY NOTES	12. SPONSORING MILITARY ACTIVITY
	U. S. Army Electronics Command Electronic Warfare Lab., AMSEL-WL-S Fort Monmouth, N. J. 07703

13. ABSTRACT Three nonlinear models for function transistors are shown to be equivalent, physically. Their differences lie in the state variables employed. The incremental behavior of these models is compared with that of the Hybrid-π and high frequency tee.

The computational utility of the voltage-controlled and the charged-controlled models are compared for a switching circuit example. If a single model is used to describe the transistor, all models are "strongly" nonlinear in one or more operating regions. In any single operating region, however, an appropriate model choice leads to "almost linear" equations.

DD FORM 1 JAN 64 1473

UNCLASSIFIED

Security Classification

14. KEY WORDS	LINK A		LINK B		LINK C	
	ROLE	WT	ROLE	WT	ROLE	WT

INSTRUCTIONS

1. ORIGINATING ACTIVITY: Enter the name and address of the contractor, subcontractor, grantee, Department of Defense activity or other organization *(corporate author)* issuing the report.

2*a*. REPORT SECURITY CLASSIFICATION: Enter the overall security classification of the report. Indicate whether "Restricted Data" is included. Marking is to be in accordance with appropriate security regulations.

2*b*. GROUP: Automatic downgrading is specified in DoD Directive 5200.10 and Armed Forces Industrial Manual. Enter the group number. Also, when applicable, show that optional markings have been used for Group 3 and Group 4 as authorized.

3. REPORT TITLE: Enter the complete report title in all capital letters. Titles in all cases should be unclassified. If a meaningful title cannot be selected without classification, show title classification in all capitals in parenthesis immediately following the title.

4. DESCRIPTIVE NOTES: If appropriate, enter the type of report, e.g., interim, progress, summary, annual, or final. Give the inclusive dates when a specific reporting period is covered.

5. AUTHOR(S): Enter the name(s) of author(s) as shown on or in the report. Enter last name, first name, middle initial. If military, show rank and branch of service. The name of the principal author is an absolute minimum requirement.

6. REPORT DATE: Enter the date of the report as day, month, year; or month, year. If more than one date appears on the report, use date of publication.

7*a*. TOTAL NUMBER OF PAGES: The total page count should follow normal pagination procedures, i.e., enter the number of pages containing information.

7*b*. NUMBER OF REFERENCES: Enter the total number of references cited in the report.

8*a*. CONTRACT OR GRANT NUMBER: If appropriate, enter the applicable number of the contract or grant under which the report was written.

8*b*, 8*c*, & 8*d*. PROJECT NUMBER: Enter the appropriate military department identification, such as project number, subproject number, system numbers, task number, etc.

9*a*. ORIGINATOR'S REPORT NUMBER(S): Enter the official report number by which the document will be identified and controlled by the originating activity. This number must be unique to this report.

9*b*. OTHER REPORT NUMBER(S): If the report has been assigned any other report numbers *(either by the originator or by the sponsor)*, also enter this number(s).

10. AVAILABILITY/LIMITATION NOTICES: Enter any limitations on further dissemination of the report, other than those imposed by security classification, using standard statements such as:

(1) "Qualified requesters may obtain copies of this report from DDC."

(2) "Foreign announcement and dissemination of this report by DDC is not authorized."

(3) "U. S. Government agencies may obtain copies of this report directly from DDC. Other qualified DDC users shall request through

_____."

(4) "U. S. military agencies may obtain copies of this report directly from DDC. Other qualified users shall request through

_____."

(5) "All distribution of this report is controlled. Qualified DDC users shall request through

_____."

If the report has been furnished to the Office of Technical Services, Department of Commerce, for sale to the public, indicate this fact and enter the price, if known.

11. SUPPLEMENTARY NOTES: Use for additional explanatory notes.

12. SPONSORING MILITARY ACTIVITY: Enter the name of the departmental project office or laboratory sponsoring *(paying for)* the research and development. Include address.

13. ABSTRACT: Enter an abstract giving a brief and factual summary of the document indicative of the report, even though it may also appear elsewhere in the body of the technical report. If additional space is required, a continuation sheet shall be attached.

It is highly desirable that the abstract of classified reports be unclassified. Each paragraph of the abstract shall end with an indication of the military security classification of the information in the paragraph, represented as *(TS), (S), (C), or (U)*.

There is no limitation on the length of the abstract. However, the suggested length is from 150 to 225 words.

14. KEY WORDS: Key words are technically meaningful terms or short phrases that characterize a report and may be used as index entries for cataloging the report. Key words must be selected so that no security classification is required. Identifiers, such as equipment model designation, trade name, military project code name, geographic location, may be used as key words but will be followed by an indication of technical context. The assignment of links, rules, and weights is optional.